CAMBRIDGE
UNIVERSITY PRESS

Review Article

Influence of excess alumina on mullite synthesized from pyrophyllite by spark plasma sintering

Rasidi Sule[1]* 🆔 and Iakovos Sigalas[2,3]

[1]Nanotechnology and Water Sustainability Research Unit, College of Science, Engineering & Technology, University of South Africa, Florida Science Campus, Johannesburg, South Africa; [2]DST-NRF Centre of Excellence in Strong Materials, University of Witwatersrand, Johannesburg, South Africa and [3]School of Chemical and Metallurgical Engineering, University of the Witwatersrand, Johannesburg, South Africa

Abstract

The influence of excess Al_2O_3 on 3:2 mullite produced from α-Al_2O_3 and pyrophyllite powder was examined. A mixture consisting of 28 wt.% dehydroxylated pyrophyllite and 72 wt.% α-Al_2O_3 was milled in an attrition mill. The milled powders were sintered by spark plasma sintering (SPS) at 1600°C for 10, 20 and 30 min. Subsequently, the samples were heated at 1350°C for 2 h to determine the influence of the excess Al_2O_3 on the microstructure. No glassy phase was detected in the sample containing 72 wt.% Al_2O_3 and sintered at 1600°C for 20 min. The sample with 72 wt.% Al_2O_3 had greater hardness and fracture toughness compared to 3:2 mullite. The greatest hardness and fracture toughness of 12.43 GPa and 2.71 MPa m$^{-0.5}$, respectively, were obtained in the sample containing 72 wt.% Al_2O_3 sintered at 1600°C for 20 min.

Aluminosilicates have been used widely in mullite ceramic industries due to their unique combination of alumina (Al_2O_3) and silica (SiO_2) (Aksel, 2003; Yahya *et al.*, 2016). Because of its excellent mechanical stability, low thermal expansion, low thermal conductivity, excellent creep resistance, high-temperature strength and good chemical stability, mullite has found applications in the steel and glass manufacturing industries, as well as in microelectronic packaging (Kool *et al.*, 2015; Schneider *et al.*, 2015; Saeidabadi *et al.*, 2018).

The mullite produced from aluminosilicates such as kyanite, andalusite and sillimanite decomposes to produce 3:2 mullite and an SiO_2 polymorph at temperatures ranging from 1400°C to 1600°C due to excess SiO_2 in the mineral (Kool *et al.*, 2015). This excess SiO_2 may react with mineral impurities to form an undesired phase, which might affect adversely the product quality (Aguilar-Santillan *et al.*, 2007). Previous studies have shown that the presence of a glassy phase in mullite prepared from aluminosilicate ceramic materials is detrimental to its mechanical properties and so limits its structural applications (Aksay *et al.*, 1991; Chen *et al.*, 2000). The addition of excess Al_2O_3 may eliminate the possible formation of free SiO_2, thereby producing a mullite–Al_2O_3 (MA) composite with improved quality (Tripathi *et al.*, 2001).

The use of pyrophyllite ($Al_2Si_4O_{10}(OH)_2$) in the production of mullite ceramics is limited (Mukhopadhyay *et al.*, 2011; Sule & Sigalas, 2018). This might be attributed to the impurities present in the natural pyrophyllite, which might influence its properties and behaviour during sintering (Mukhopadhyay *et al.*, 2010).

Nevertheless, pyrophyllite may be a partial replacement for china clay and a viable alternative for kaolinite in end products where mullite is the desirable phase (Mukhopadhyay *et al.*, 2010).

Previous studies have shown that ceramic products such as AL97ML in the armour systems manufacturing industry with Al_2O_3 contents ranging from 72 to 76 wt.%, containing either mullite or other aluminosilicates, would result in excellent mechanical properties (Sadik *et al.*, 2014). Medvedovski *et al.* (2006) also reported that MA ceramic composites containing small amounts of glassy phases would have better ceramic properties than pure mullite or pyrophyllite unless the Al_2O_3 content exceeds 98 wt.%. On the other hand, various studies are available on the improvement of the densification and mechanical properties of mullite with the addition of Al_2O_3, ZrO_2 and SiC (Gao *et al.*, 2002; Khor *et al.*, 2003; Cascales *et al.*, 2015). Aguilar-Santillan *et al.* (2007) investigated the effect of attrition-milled kyanite and Al_2O_3 on mullite. They reported that attrition milling decreases the kyanite decomposition temperature and promotes the reaction of added Al_2O_3 with released SiO_2 to form secondary mullite with a greater density. However, very limited information is available on the control of the glassy phase during the synthesis of mullite derived from the mixture of pyrophyllite and Al_2O_3 with improved microstructural and mechanical properties. In order to find a solution to this problem, significant amounts of Al_2O_3 were incorporated in a stoichiometric mullite composition to produce a MA product.

Previous works have reported on the synthesis of mullite and MA products from natural aluminosilicate minerals using conventional processing and sintering methods (Yamuna *et al.*, 2002; Yan *et al.*, 2010). However, significant energy consumption during sintering necessitates the use of novel sintering techniques. Recently, spark plasma sintering (SPS) has been used in the
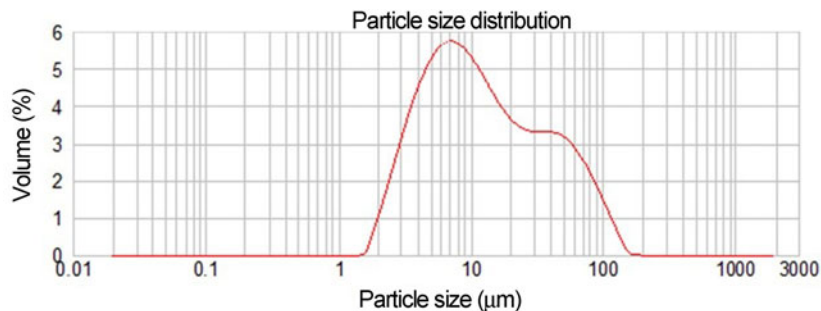
Table 1. Chemical composition (wt.%) of as-received pyrophyllite powder (Sule & Sigalas, 2018).

| SiO_2	Al_2O_3	Fe_2O_3	FeO	MnO	MgO	CaO	Na_2O	K_2O	TiO_2	P_2O_5	Cr_2O_3	LOI
58.63	30.30	0.12	0.99	0.01	0.07	0.05	0.17	1.09	1.90	0.15	0.03	6.06

LOI = loss on ignition.

Fig. 1. Particle-size distribution of as-received pyrophyllite powder; $d_{10} = 3.32\,\mu m$, $d_{50} = 9.42\,\mu m$, $d_{90} = 45.05\,\mu m$.

fabrication of mullite (Zhang *et al.*, 2009; Ghahremani *et al.*, 2015). This technique is known to produce very dense ceramic materials with controlled grain growth (Suárez *et al.*, 2013). A previous study by the present authors showed that the SPS technique might be used to produce mullite from a mixture of pyrophyllite and α-Al_2O_3 (Sule & Sigalas, 2018). An effort is therefore made to investigate the influence of excess α-Al_2O_3 powder on the microstructure, hardness and fracture toughness of MA produced from a pyrophyllite–Al_2O_3 mixture with respect to the firing time.

Materials and methods

Sample preparation

The pyrophyllite powder used in this study was mined in Ottosdal in South Africa (supplied by Wonderstone, Ltd), and the reactive α-Al_2O_3 (P172SB: 99.7% purity) was added to produce samples of MA. The particle size was measured using a Malvern Mastersizer particle-size analyser. The as-received pyrophyllite powder had an average particle size of <63 μm and the powder was milled to 0.5 μm. PANalytical X-ray fluorescence (model AXIOS mAX spectrometer at 50 kV and 50 mA) was used to characterize the mineralogy of the pyrophyllite powder. Then, the milled powder was fired in a furnace at 800°C for 30 min to produce a dehydroxylated pyrophyllite powder. The crystalline water molecules of phyllosilicates, including pyrophyllite, serpentine, talc and kaolinite, are lost during dehydration (Taylor, 1962). The chemical reaction of stoichiometric mullite composition from fired pyrophyllite and Al_2O_3 powder was expressed as:

$$x(Al_2O_3 \cdot 4SiO_2) + yAl_2O_3 = 1.2(3Al_2O_3 \cdot 2SiO_2) \qquad (1)$$
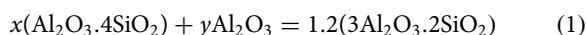
where $x = 0.6$ and $y = 3.0$.

Two different powder samples were synthesized: the first sample is 3:2 mullite powder that contains 40 wt.% dehydroxylated pyrophyllite and 60 wt.% Al_2O_3. The second powder sample was produced from 72 wt.% Al_2O_3 and 28 wt.% dehydroxylated pyrophyllite. The powders were mixed until homogeneous in an attrition mill using isopropanol and Al_2O_3 balls as milling media. The mixed powder (i.e. powder obtained after milling pyrophyllite and Al_2O_3 for 6 h) was oven dried at 60°C, and a 90 μm sieve was used to break down the soft agglomerates. A HPD5 SPS machine

(FCT Systeme GmbH) was used to consolidate the powder. A pressure of 50 MPa was applied throughout the sintering cycle at 1600°C with heating rates of 100°C min^{-1} and soaking times of 10, 20 and 30 min, respectively. Furthermore, the sample was heated at 1350°C for 2 h to examine the effect of excess Al_2O_3 on microstructure.

Characterization of the sintered products

Phase identification was performed on the sintered specimen using X-ray diffraction (XRD; Bruker D2 Advance diffractometer at Wits University). Traces were collected over the 2θ range between 10° and 90° at room temperature (Cu radiation at 30 kV and 10 mA). The densities of the sintered samples were measured using the Archimedes principle. The samples were thermally etched at 1350°C and coated with a combination of carbon and gold–palladium. A field emission scanning electron microscope (FESEM; Carl Zeiss Sigma) was used to examine the microstructure of the polished surface. A Vickers hardness tester (FM 700) was employed to measure the hardness and fracture toughness of the sintered samples using the indentation technique at a load of 5 kg for 10 s. The fracture toughness was calculated according to the technique described by Anstis *et al.* (1981). The samples were measured five times and the average values were reported.

Results and discussion

Characterization and densification of sintered samples

The as-received pyrophyllite powder contained 58.63 wt.% SiO_2 and 30.30 wt.% Al_2O_3 with minor amounts of Fe_2O_3, FeO, TiO_2 and K_2O (Table 1). Figure 1 shows the particle-size distribution of the as-received pyrophyllite powder. The average particle size was 9.42 μm, which was reduced to 0.20 μm in mixed powder after 6 h of milling. The mineralogical composition of the as-received pyrophyllite powder was reported by Sule & Sigalas (2018). The XRD analysis was used to identify the phases present in the mixture of 72 wt.% Al_2O_3 and 28 wt.% pyrophyllite powder. Al_2O_3, dehydroxylated pyrophyllite and minor quartz were the dominant phases (Fig. 2). A small fraction of pyrophyllite was converted to an amorphous phase due to the structural disorder during milling (Kim *et al.*, 2014).
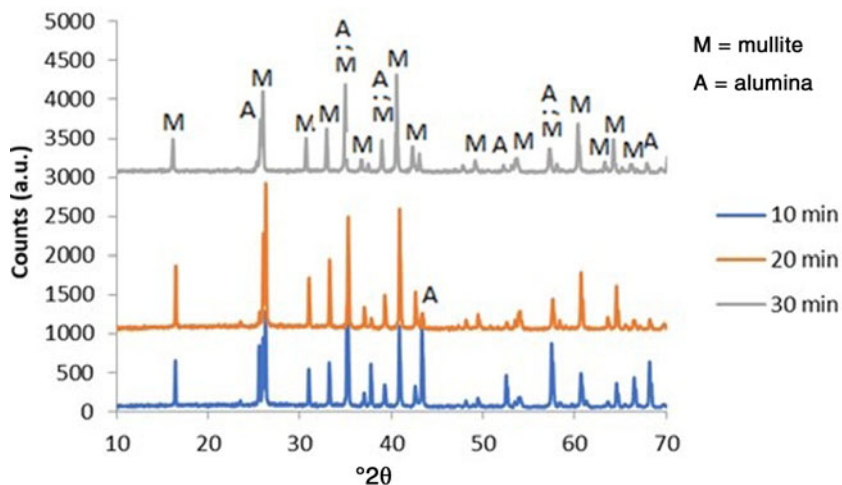
In order to examine the effect of excess Al_2O_3 on stoichiometric 3:2 mullite, three samples containing excess Al_2O_3 were
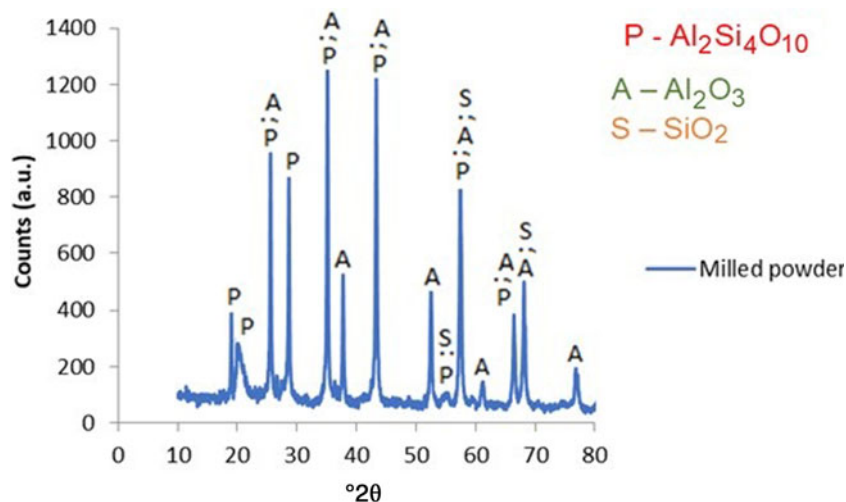
Fig. 2. XRD trace of milled 72 wt.% Al_2O_3 and 28 wt.% pyrophyllite powder.
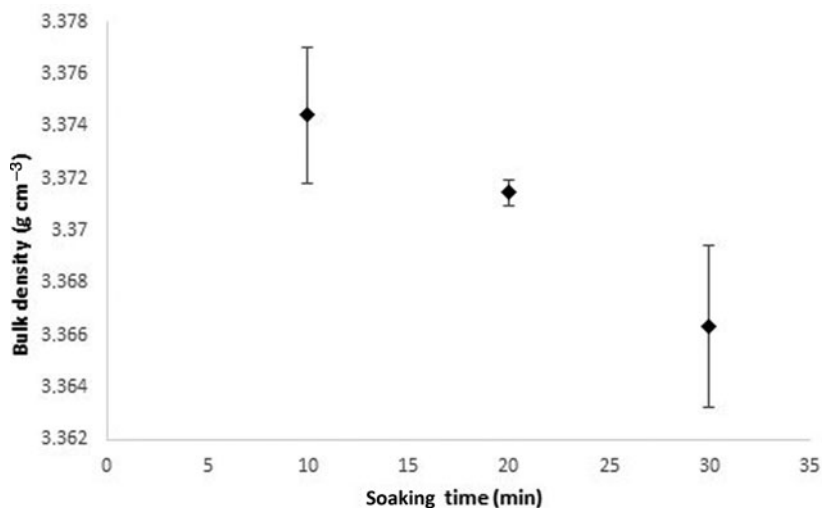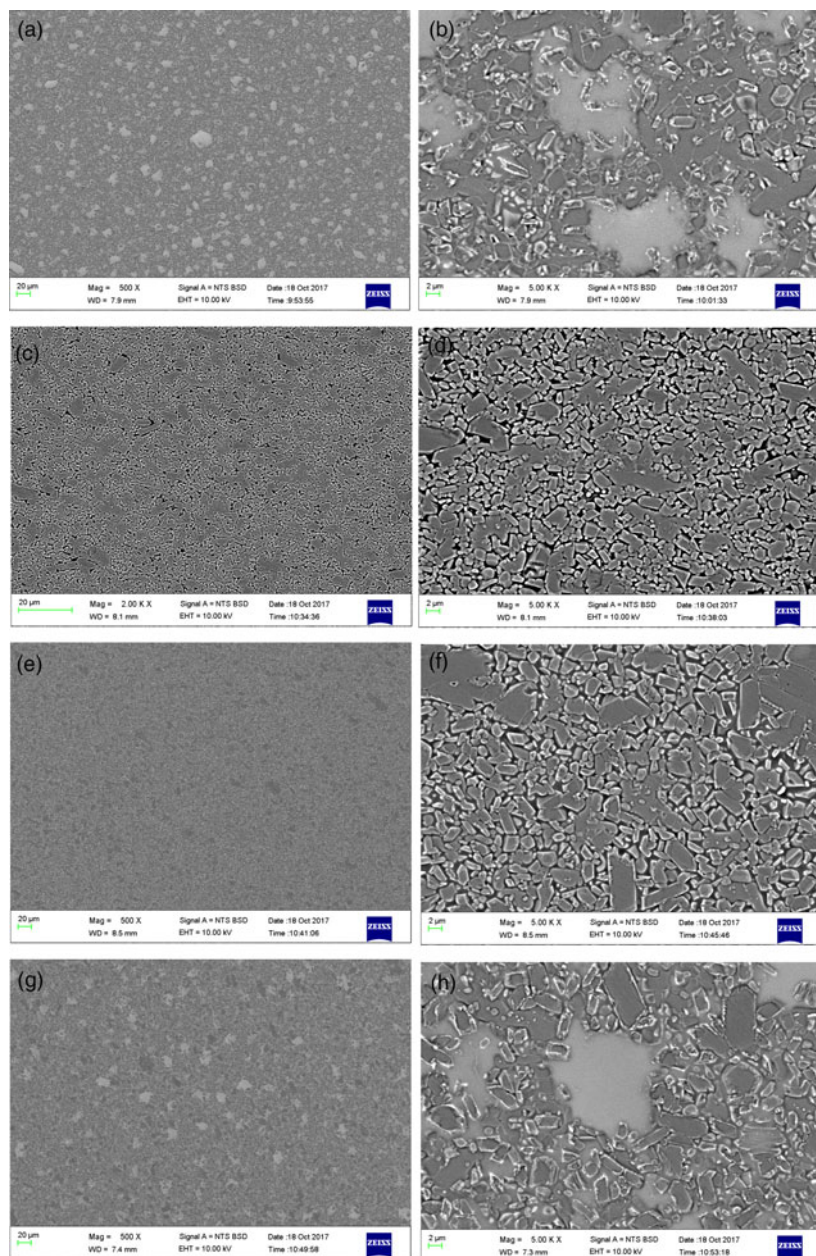

Fig. 3. Effect of soaking time on sintered MA density at 1600°C.

Fig. 4. XRD traces of MA samples sintered at 1600°C with progressive soaking times of 10, 20 and 30 min.

produced at 1600°C with various soaking times of 10, 20 and 30 min. Bulk densities of 3.374, 3.371 and 3.366 g cm^{-3} were obtained for MA mixtures sintered for 10, 20 and 30 min, respectively. These density values were greater than the density

of 3.16 g cm^{-3} obtained for 3:2 mullite sintered at 1600°C for varying soaking times (Sule & Sigalas, 2018). The increase in density of MA samples might be attributed to the fact that Al_2O_3 has a greater theoretical density of 3.95 g cm^{-3} (Olszyna

Fig. 5. SEM images of (a,b) mullite samples sintered at 1600°C for 20 min, (c,d) MA sintered for 10 min, (e,f) MA sintered for 20 min and (g,h) MA sintered for 30 min.

et al., 1997). Figure 3 shows the effect of soaking time on bulk density in excess Al_2O_3 samples sintered at 1600°C. The sample density decreases slightly with an increase in soaking time. This might be attributed to Al_2O_3 reacting with the SiO_2 from thermally decomposed dehydroxylated pyrophyllite to produce 3:2 mullite over time (Mukhopadhyay et al., 2010).

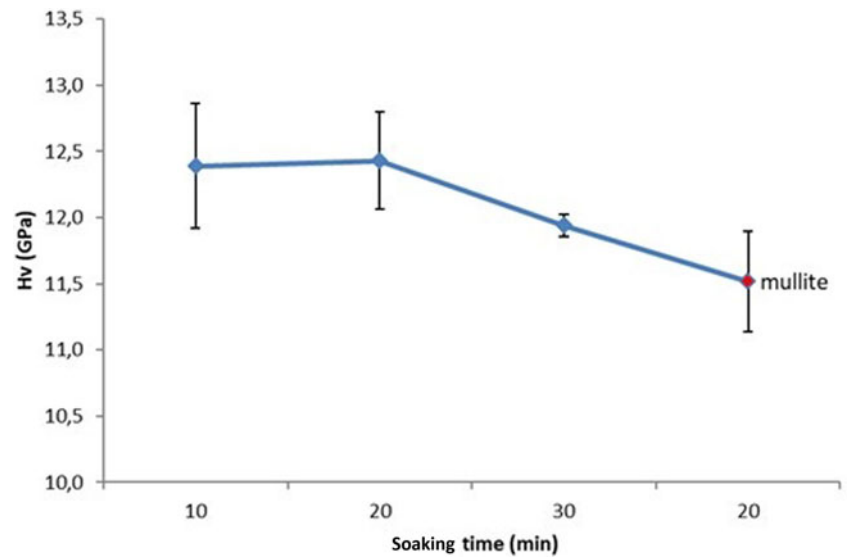The XRD traces of samples sintered at 1600°C with various soaking times is shown in Fig. 4. No other phases apart from mullite and Al_2O_3 were observed. The relative intensities of the mullite peaks increased and those of the Al_2O_3 peaks decreased for the samples produced after 20 and 30 min.

Microstructure evolution

Figure 5a,b shows micrographs of 3:2 mullite sintered at 1600°C for 20 min, while Fig. 5c–h shows micrographs of MA mixtures fired for 10, 20 and 30 min. Typical equiaxial grain structures were observed in the mullite sample. The MA sample sintered for 10 min shows mixed acicular and equiaxial grains with spaces between the grains. The MA sample sintered for 20 min revealed an equiaxial grain structure similar to that of the mullite sample. In addition, the grains of the MA sample sintered for 20 min were packed more closely than those of the 10 min MA sample. The Joule heating effect of the SPS might enhance the densification in the MA sample sintered for 20 min (Ghahremani et al., 2015). However, there is a slight increase in the grain size of the MA sample produced after 20 min of sintering, which might be attributed to the longer soaking time. By contrast, the sample sintered for 30 min contains a glassy phase with refined equiaxial grains. The morphologies of the mullite sample sintered for 20 min and that of MA sintered for 30 min were different. The excess Al_2O_3 in the 30 min sample decreased the glassy phase content considerably. This suggests that the glassy phase, attributed to the impurities that limit the structural properties of

Fig. 6. Vickers hardness (Hv) at room temperature of the MA samples sintered at 1600°C with progressive soaking times of 10, 20 and 30 min.

Fig. 7. Fracture toughness at room temperature of the MA samples sintered at 1600°C with progressive soaking times of 10, 20 and 30 min.
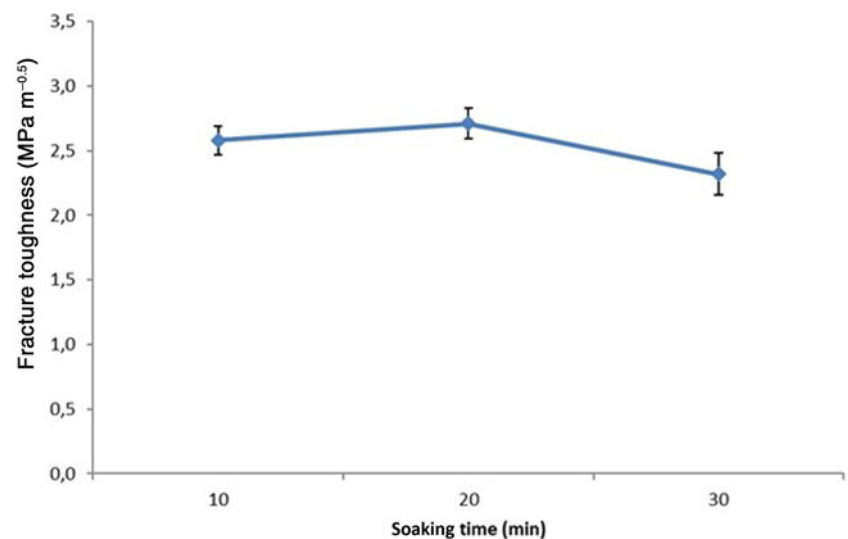
mullite product synthesized from the pyrophyllite and Al_2O_3 mixture, might be eliminated.

Mechanical properties

A Vickers hardness value of 12.39 ± 0.47 GPa was observed for the sample sintered at 1600°C for 10 min. The hardness value increased slightly when the soaking time increased from 10 to 20 min, but it decreased at soaking times of 30 min. Hardness values of 12.43 ± 0.37 and 11.94 ± 0.08 GPa were obtained for 20 and 30 min soaking times, respectively. The microstructural features of the samples corroborated the hardness results obtained in this study. The MA samples sintered for 10 and 20 min soaking times have the same Vickers hardness values within measurement error. However, the hardness of the MA sample sintered for 30 min was slightly lower, but higher than that of the 3:2 mullite sample (11.52 ± 0.38 GPa) (Sule & Sigalas, 2018). Cascales *et al.* (2015) reported on the mechanical properties of mullite and MA produced by SPS. In that study, the MA sample has a hardness of 13.5 ± 0.1 GPa, which is slightly higher than that of mullite (12.5 ± 0.1 GPa)

due to the presence of Al_2O_3. Figure 6 shows the influence of soaking time on the hardness of the samples.

Figure 7 depicts the fracture toughness (K_{IC}) of the MA samples as a function of soaking time. An increase in soaking time resulted in a slight increase in fracture toughness. After 10 min of soaking time, the sample produced a fracture toughness of 2.58 MPa $m^{-0.5}$, whilst after 20 and 30 min soaking times, the samples displayed fracture toughness values of 2.71 and 2.32 MPa $m^{-0.5}$, respectively. A fracture toughness of 1.97 MPa $m^{-0.5}$ was obtained for the 3:2 mullite sample. The greatest fracture toughness value was obtained for a 20 min soaking time. The hardness and fracture toughness values of the MA samples were greater than those of the stoichiometric 3:2 mullite samples due to the presence of excess Al_2O_3. Previous reports have shown that the fracture toughness of mullite produced from kaolin and Al_2O_3 increases with an increase in Al_2O_3 content (Chen *et al.*, 2000; Cascales *et al.*, 2015). On the other hand, the fracture toughness of the MA synthesized in this work is slightly greater than that reported for a SiC–mullite nanocomposite prepared by SPS (Khor *et al.*, 2003). The density, hardness and fracture surface suggest

that the pyrophyllite–Al$_2$O$_3$ composition with 72 wt.% Al$_2$O$_3$ sintered at 1600°C should be kept for a 20 min soaking time. This would prevent the specimens from having poorer mechanical properties due to the formation of a glassy phase, which may occur as a result of prolonged heating.

Conclusion

This study confirmed that MA ceramics with attractive mechanical properties might be formed through the sintering of a pyrophyllite and α-Al$_2$O$_3$ mixture using SPS. The microstructure of the MA produced after a 20 min soaking time indicated that no glassy phase was present. The hardness and fracture toughness values of the MA consolidated by SPS showed superior strength compared to that of pure mullite. The optimal sintering conditions for MA ceramics synthesized from a pyrophyllite and Al$_2$O$_3$ mixture were a sintering temperature of 1600°C and a 20 min soaking time.

Conflict of interest. None.

References

Aguilar-Santillan J., Balmori-Ramirez H. & Bradt, R.C. (2007) Dense mullite from attrition milled kyanite and alpha-alumina. *Journal of Ceramic Processing Research*, **8**, 1–11.

Aksay I.A., Dabbs D.M. & Sarikaya M. (1991) Mullite for structural, electronic, and optical applications. *Journal of the American Ceramic Society*, **74**, 2343–2358.

Aksel C. (2003) The effect of mullite on the mechanical properties and thermal shock behaviour of alumina–mullite refractory materials. *Ceramics International*, **29**, 183–188.

Anstis G., Chantikul P., Lawn B.R. & Marshall D. (1981) A critical evaluation of indentation techniques for measuring fracture toughness: I, direct crack measurements. *Journal of the American Ceramic Society*, **64**, 533–538.

Cascales A., Tabares N., Bartolomé J.F., Cerpa A., Smirnov A., Moreno R. & Nieto M.I. (2015) Processing and mechanical properties of mullite and mullite–alumina composites reinforced with carbon nanofibers. *Journal of European Ceramic Society*, **35**, 3613–3621.

Chen C., Lan G. & Tuan W. (2000) Preparation of mullite by the reaction sintering of kaolinite and alumina. *Journal of the European Ceramic Society*, **20**, 2519–2525.

Gao L., Jin X., Kawaoka H., Sekino, T. & Niihara, K. (2002) Microstructure and mechanical properties of SiC–mullite nanocomposite prepared by spark plasma sintering. *Materials Science and Engineering: A*, **334**, 262–266.

Ghahremani D., Ebadzadeh T. & Maghsodipour, A. (2015) Spark plasma sintering of mullite: relation between microstructure, properties and spark plasma sintering (SPS) parameters. *Ceramics International*, **41**, 6409–6416.

Khor K.A., Yu L., Li Y., Dong Z.L. & Munir, Z. (2003) Spark plasma reaction sintering of ZrO$_2$–mullite composites from plasma spheroidized zircon/alumina powders. *Materials Science and Engineering: A*, **339**, 286–296.

Kim W., Chae W., Kwon S., Kim K., Lee H. & Kim S. (2014) Effect of dry grinding of pyrophyllite on the hydrothermal synthesis of zeolite Na-X and Na-A. *Materials Transactions*, **99**, 1488–1493.

Kool A., Thakur P., Bagch, B., Hoque, N.A. & Das, S. (2015) Mechanical, dielectric and photoluminescence properties of alumina–mullite composite derived from natural Ganges clay. *Applied Clay Science*, **114**, 349–358.

Medvedovski, E. (2006) Alumina–mullite ceramics for structural applications. *Ceramics International*, **32**, 369–375.

Mukhopadhyay, T.K., Dana, K. & Ghatak, S. (2011). Pyrophyllite-a potential material for application in tri-axial porcelain systems. *Industrial Ceramics*, **31**, 165–173.

Mukhopadhyay T.K., Ghatak S. & MaitI, H.S. (2010) Pyrophyllite as raw material for ceramic applications in the perspective of its pyro-chemical properties. *Ceramics International*, **36**, 909–916.

Olszyna A., Marchlewski P. & Kurzydłowski K. (1997) Sintering of high-density, high-purity alumina ceramics. *Ceramics International*, **23**, 323–328.

Sadik C., Amrani I.-E.E. & Albizane A. (2014) Processing and characterization of alumina–mullite ceramics. *Journal of Asian Ceramic Societies*, **2**, 310–316.

Saeidabadi E.K., Ebadzadeh T. & Salahi E. (2018) Preparation of mullite from alumina/aluminum nitrate and kaolin clay through spark plasma sintering process. *Ceramics International*, **44**, 21053–21066.

Schneider H,, Fischer R.X. & Schreuer J. (2015) Mullite: crystal structure and related properties. *Journal of the American Ceramic Society*, **98**, 2948–2967.

Suárez M., Fernández A., Menéndez J., Torrecillas R., Kessel H., Hennicke J. *et al.* (2013) Challenges and opportunities for spark plasma sintering: a key technology for a new generation of materials. *Sintering Applications*, **13**, 319–342.

Sule R. & Sigalas I. (2018) Effect of temperature on mullite synthesis from attrition-milled pyrophyllite and α-alumina by spark plasma sintering. *Applied Clay Science*, **162**, 288–296.

Taylor H. (1962) Homogeneous and inhomogeneous mechanisms in the dehydroxylation of minerals. *Clay Minerals Bulletin*, **5**, 45–55.

Tripathi H.S., Das S., Mukherjee B., Ghosh, A. & Banerjee G. (2001) Synthesis and thermo-mechanical properties of mullite–alumina composite derived from sillimanite beach sand: effect of ZrO$_2$. *Ceramics International*, **27**, 833–837.

Yahya H., Othman M.R. & Ahmad Z.A. (2016) Effect of mullite formation on properties of aluminosilicate ceramic balls. *Procedia Chemistry*, **19**, 922–928.

Yamuna A., Devanarayanan S. & Lalithambika M. (2002) Phase-pure mullite from kaolinite. *Journal of the American Ceramic Society*, **85**, 1409–1413.

Yan W., Li N. & Han B. (2010) Effects of sintering temperature on pore characterisation and strength of porous corundum–mullite ceramics. *Journal of Ceramic Processing Research*, **11**, 388–391.

Zhang G., Wang Y., Fu Z., Wang H., Wang W., Zhang J. *et al.* (2009) Transparent mullite ceramic from single-phase gel by spark plasma sintering. *Journal of the European Ceramic Society*, **29**, 2705–2711.